ACCRETION TORQUES AND MOTION OF THE HOT SPOT ON THE ACCRETING MILLISECOND PULSAR XTE J1807-294

Citation: Patruno, Alessandro et al. "ACCRETION TORQUES AND MOTION OF THE HOT SPOT ON THE ACCRETING MILLISECOND PULSAR XTE J1807-294." The Astrophysical Journal 717, 2 (June 2010): 1253–1261 © 2010 American Astronomical Society

As Published: http://dx.doi.org/10.1088/0004-637X/717/2/1253

Publisher: American Astronomical Society/IOP Publishing

Persistent URL: http://hdl.handle.net/1721.1/116456

Version: Final published version: final published article, as it appeared in a journal, conference proceedings, or other formally published context

The Astrophysical Journal, 717:1253–1261, 2010 July 10 doi:10.1088/0004-637X/717/2/1253

ACCRETION TORQUES AND MOTION OF THE HOT SPOT ON THE ACCRETING MILLISECOND PULSAR XTE J1807−294

Alessandro Patruno[1], Jacob M. Hartman[2], R. Wijnands[1], Deepto Chakrabarty[3], and Michiel van der Klis[1]
[1] Astronomical Institute "Anton Pannekoek," University of Amsterdam, Science Park 904, 1098 XH Amsterdam, The Netherlands; a.patruno@uva.nl
[2] Space Science Division, Naval Research Laboratory, Washington, DC 20375, USA
[3] Department of Physics and Kavli Institute for Astrophysics and Space Research, Massachusetts Institute of Technology, Cambridge, MA 02139, USA
Received 2009 February 13; accepted 2010 May 21; published 2010 June 23

ABSTRACT

We present a coherent timing analysis of the 2003 outburst of the accreting millisecond pulsar (AMXP) XTE J1807−294. We find a 95% confidence interval for the pulse frequency derivative of $(+0.7, +4.7)\times10^{-14}$ Hz s^{-1} and $(-0.6, +3.8)\times10^{-14}$ Hz s^{-1} for the fundamental and second harmonics, respectively. The sinusoidal fractional amplitudes of the pulsations are the highest observed among AMXPs and can reach values of up to 27% (2.5–30 keV). The pulse arrival time residuals of the fundamental frequency follow a linear anti-correlation with the fractional amplitudes that suggests hot spot motion both in longitude and latitude over the surface of the neutron star. An anti-correlation between residuals and X-ray flux suggests an influence of the accretion rate on pulse phase and casts doubts on the interpretation of pulse frequency derivatives in terms of changes of spin rates and torques on the neutron star.

Key words: stars: individual (XTE J1807−294) – stars: neutron – X-rays: stars

Online-only material: color figures

1. INTRODUCTION

An open problem in the field of accreting millisecond pulsars (AMXPs) is how to devise a reliable method to measure spin and orbital parameters. Since the discovery of the first AMXP (Wijnands & van der Klis 1998), considerable improvements have been made, leading to the measurement of accurate orbital and pulse frequency parameters for 12 of the 13 known AMXPs (see Wijnands 2004; Poutanen 2006 for a review). Current methods (e.g., Taylor 1992) are based on folding procedures to reconstruct the pulse profiles of the accreting neutron star and on the direct measurement of the pulse phase variations due to orbital Doppler shift and pulse frequency changes (for example due to torques). The pulse phases are fitted using χ^2 minimization techniques. However, a substantial complication sometimes arises due to the presence of a strong unmodeled noise component in the pulse phases that, when ignored, affects the reliability of the parameters derived.

Two possible strategies have been used in the literature to try and overcome this: (1) harmonic data selection (Burderi et al. 2006; Riggio et al. 2008; Chou et al. 2008; Papitto et al. 2007) and (2) the use of a minimum variance estimator (Boynton & Deeter 1985; Hartman et al. 2008; Hartman et al. 2009). In the first case, the pulse profiles are decomposed into their harmonic components—generally one sinusoid at the fundamental frequency (or first harmonic, ν) and one at the second harmonic (2ν)—and are analyzed separately, measuring two independent sets of orbital and spin parameters. The harmonic with the weakest noise content is selected for the measurement of the pulse frequency and the noisier one is discarded (e.g., Burderi et al. 2006). Although this use of the most "stable" harmonic reduces the χ^2, this selection throws away part of the information and in that sense is not optimal. The hypothesis behind the selection of the most stable harmonic is that, for unknown reasons, that harmonic tracks the spin of the neutron star better. Burderi et al. (2006) speculated that the second harmonic might be more stable because it arises from accretion onto both the polar caps and hence is insensitive to the flux ratio between poles. Recently, Patruno et al. (2010) found an AMXP (*Swift* J1756.9−2508) whose second harmonic was *less* stable than the fundamental, casting doubts on this interpretation. Furthermore, it should be noted that a low level of noise in the pulse phases is not in itself evidence that the pulse frequency accurately tracks the neutron star *spin frequency*. The *pulse frequency* and its time derivatives are indeed observables, while the spin frequency and derivatives are not. Pulse frequency and spin frequency can be different if, for example, the hot spot has a non-zero velocity with respect to the neutron star surface.

In the second method, both harmonics are used and weighted to minimize the effect of phase noise (Boynton & Deeter 1985; Hartman et al. 2008). However, in this second situation data selection in practice is also performed. If the phases of both harmonics change differently, the possibility of defining pulse arrival times breaks down and the data where this happens have to be excluded from the analysis (Hartman et al. 2008). Because both methods employ different data selections, different results are obtained when analyzing the same source. For example, in the case of SAX J1808.4−3658, the pulse frequency derivative $\dot{\nu}$ measured from only the second harmonic was 4.4×10^{-13} Hz s^{-1} for the first 14 days of the 2002 outburst and -7.6×10^{-14} Hz s^{-1} for the rest of the outburst (Burderi et al. 2006). In Hartman et al. (2008), we considered the same source and gave an upper limit of $|\dot{\nu}| < 2.5\times10^{-14}$ Hz s^{-1} for all four outbursts for which high-resolution timing data were available. The reason for this discrepancy is that while Burderi et al. (2006) used only the information carried by the second harmonic and rejected the results of the fundamental frequency, we used both harmonics but excluded the initial data where the phase variations were stronger and discrepant between harmonics (Hartman et al. 2008). So, these differences arise as a consequence of different data selections.

To address this problem, we present in this paper a detailed study of all sources of uncertainty that need to be taken into

account when measuring the neutron star spin parameters. In Section 2, we explain the data reduction and introduce the method used to measure the pulse phases. In Section 3.1, we explain the Monte Carlo (MC) method used to calculate realistic statistical errors when the pulse phases are affected by timing noise. A similar approach was already presented in Hartman et al. (2008). In Section 3.2, we investigate to what extent the pulse phase variations are more or less correlated with the X-ray luminosity. The results found so far in other sources (Patruno et al. 2009) are in contrast with standard accretion theory and indicate that it is the pulse phase rather than the pulse frequency derivative that correlates to the X-ray luminosity. An initial analysis of these kind of phase–flux correlations was reported by Riggio et al. (2008) for XTE J1807−294. A first attempt to explain the phenomenon was given by Lamb et al. (2009), who proposed a wandering hot spot on the neutron star surface at the origin of the phase–flux variations. In this sense, we try to better characterize the timing noise as observed in AMXPs focusing on a source where the noise is strong: XTE J1807−294 (henceforth referred to as J1807) which has been in outburst for ≈120 days in 2003 (Markwardt et al. 2003). In Section 3.3, we focus on the properties of the pulse profiles of J1807, on their harmonic content and on the pulse amplitudes. We investigate whether the presence of timing noise is related in some way to the pulsed fractions. Some models that try to explain timing noise in AMXPs predict a connection between these two quantities. For example, a motion of the hot spot produces both variations in phase and pulse amplitudes (Lamb et al. 2009). In Section 3.4, we test the standard accretion theory: short-term $\dot{\nu}$ measurements need to be related to X-ray flux variations (see, for example, Bildsten et al. 1997). In Section 4, we discuss all these findings and provide a first evidence for the origin of timing noise as a motion of the hot spot on the neutron star surface. In Section 5, we outline our conclusions.

2. DATA REDUCTION AND RECONSTRUCTION OF THE PULSE PROFILES

We reduced all the pointed observations from the *RXTE* satellite taken with the proportional counter array (PCA; Jahoda et al. 2006) that cover the 2003 outburst of J1807. The PCA instrument provides an array of five proportional counter units with a collecting area of 1200 cm^2 per unit operating in the 2–60 keV range and a field of view with an FWHM of ∼1°. We constructed the X-ray light curve using the counts in PCA absolute channels 5–67 (≈2.5–30 keV). Our pulse profiles are generated by folding 512 s long chunks of light curve in profiles of $N = 32$ bins, with the ephemeris of Riggio et al. (2008). In this folding process, we used the TEMPO pulsar timing program to generate a series of polynomial expansions of the ephemeris that predict the barycentered phase of each photon detected, after the modulation of the Keplerian orbit has been removed. The total number of photons detected in a single profile bin is $x_j \pm \sqrt{x_j}$, with the error calculated from counting statistics and $j = 1, \ldots, N$. Since the pulse profile shape changes throughout the outburst, it is not possible to base the analysis on a stable template profile. Therefore, we decided to analyze the pulse profile harmonic components separately.

To calculate the pulse fractional amplitudes and phases we decomposed each profile as

$$x_j = b_0 + \sum_k b_k \cos\left\{2\pi\left[\frac{k(j-0.5)}{N} - \phi_k\right]\right\} \quad (1)$$

by using standard χ^2 minimization techniques. The term b_k is the amplitude of the sinusoid representing the kth harmonic and b_0 is the unpulsed flux component. We choose the first peak of each sinusoid in the profile as the fiducial point for each harmonic. Defining the kth harmonic frequency to be $k \cdot \nu$, the unique pulse phases ϕ_k of each harmonic range from 0 to 1. The ith pulse time of arrival (TOA) of the kth harmonic is then defined as $t_{k,i} = \frac{\phi_{k,i}}{k \cdot \nu} + \Delta t_i$. Here, Δt_i is the time of the middle of the ith folded chunk. With these definitions, a positive time shift is equivalent to a lagging pulse TOA, while a negative shift corresponds to a preceding pulse TOA with respect to the model. This is the convention that will be used later to define pulse phase residuals.

The fractional sinusoidal amplitude[4] of the ith pulse profile and the kth harmonic is calculated as follows:

$$R_{i,k} = \frac{N \times b_k}{N_{\mathrm{ph},i} - B_i}, \quad (2)$$

where $N_{\mathrm{ph,i}}$ and B_i are the total number of photons and the background counts (calculated with the FTOOL *pcabackest*) in the ith pulse profile. The error on the fractional amplitude $R_{i,k}$ is calculated propagating the errors on b_k and $N_{\mathrm{ph},i}$. The error on B_i is negligible with respect to the other errors and will not be considered further. A possible systematic contribution to the background comes from the Galactic Ridge contribution (Warwick et al. 1985). However, this contribution has an effect that is always within the errors and will be neglected.

We define a pulse profile harmonic to be significant if the ratio between the amplitude b_k and its statistical error σ_{b_k} is larger than 3.3 when using a folding time of 512 s. The choice of 3.3 guarantees that the number of false detections expected when considering the global number of pulse profiles (≈850) is less than 1. The length of the folding time was then changed to 300 and 3000 s to probe different timescales (see Section 3), and the significance threshold rescaled to 3.5σ and 3σ, respectively, according to the new number of pulse profiles.

After obtaining our set of TOAs for all the significant harmonics we chose to describe the phase ϕ of the kth harmonic (we omit the k index from now on) at the barycentric reference frame, as a combination of six terms:

$$\phi(t) = \phi_L(t) + \phi_Q(t) + \phi_O(t) + \phi_M(t) + \phi_A(t) + \phi_N(t), \quad (3)$$

where $\phi_L(t)$ is a linear function of the time ($\phi_L(t) = \phi_0 + \nu t$, with ϕ_0 being an initial reference phase), $\phi_Q(t)$ is a quadratic function of time ($\phi_Q(t) = \frac{1}{2}\dot{\nu}t^2$), and $\phi_O(t)$ is the Keplerian orbital modulation component (see Groth 1975). The term $\phi_M(t)$ is the measurement error component, and is given by a set of independent values, and is normally distributed with an amplitude that can be predicted by propagating the Poisson uncertainties due to counting statistics. The term $\phi_A(t)$ is the astrometric uncertainty position error and the last term, $\phi_N(t)$, is the so-called timing noise component that defines all the phase variations that remain. The timing noise includes, but is not limited to, any phase residual that can be described as red noise and possible extra white noise in addition to that described by the measurement error component $\phi_M(t)$.

One of the key points when dealing with timing noise is how to distinguish a true spin frequency change of the neutron star

[4] In this paper, we are quoting sinusoidal fractional amplitudes, which are $\sqrt{2}$ larger than the rms fractional amplitudes.

Table 1
Timing Parameters for XTE J1807−294 (Fundamental)

Parameter	Fundamental	MC Error (68% c.l.)	Astrometric Error	Final Error
Pulse frequency, ν (Hz)	190.62350702	2×10^{-8} Hz	3×10^{-8} Hz	4×10^{-8} Hz
Pulse frequency derivative, $\dot{\nu}$ (10^{-14} Hz s^{-1})	2.7	0.7	0.7	1.0
Reference epoch (MJD)	52720.0			

Table 2
Timing Parameters for XTE J1807−294 (Second Harmonic)

Parameter	Second Harmonic	MC Error (68 % c.l.)	Astrometric Error	Final Error
Pulse frequency, ν (Hz)	190.62350706	3×10^{-8} Hz	3×10^{-8} Hz	4×10^{-8} Hz
Pulse frequency derivative, $\dot{\nu}$ (10^{-14} Hz s^{-1})	1.6	0.8	0.7	1.1
Reference epoch (MJD)	52720.0			

from an effect that mimics it. The terms ϕ_Q and ϕ_N can both be due to torques, both *not* be due to torques, or one can, while the other is not. In the first case, the torque is not constant and has a fluctuating component. In the second case, there is a process different from a torque affecting the pulse phases. In the third case, if ϕ_Q is due to a torque, it is constant, while if ϕ_N is due to a torque then the torque is not constant.

In the presence of timing noise (ϕ_N) the formal parameter errors estimated using standard χ^2 minimization techniques are not realistic estimates of the true uncertainties, as the hypothesis behind the χ^2 minimization technique is that the source of the noise is white and its amplitude can be predicted from counting statistics. In the presence of an additional source of noise, such as the timing noise, the apparently significant measurement of a parameter can simply reflect the non-realistic estimation of the parameter errors. To solve this, we adopted the technique we already employed in Hartman et al. (2008), who used MC simulations of the timing residuals to account for the effect of timing noise on the parameter errors. The technique uses the power density spectrum of the best-fit timing residuals of a $\dot{\nu}$ model, as output by TEMPO. A preliminary inspection of the Fourier transform of the best-fit timing residuals shows a uniform random distribution of the Fourier phases between 0 and 2π. Thousands of fake power density spectra are then produced, under the assumption that the Fourier amplitudes are identical to the original spectrum and with random uncorrelated Fourier phases. The Fourier frequencies are then transformed back to the time domain into fake residuals, and thousands of ν and $\dot{\nu}$ values are measured to create a Gaussian distribution of pulse frequencies and pulse frequency derivatives. The standard deviations of these distributions are the statistical uncertainties on the pulse frequency and derivative. For a detailed explanation of the method we refer to Hartman et al. (2008).

3. RESULTS

3.1. Measurement of the Pulse Frequency and Its Derivative in the Presence of Timing Noise

We fitted the phases of each harmonic with a circular Keplerian model (ϕ_O) plus a linear term (ϕ_L) and a quadratic term (ϕ_Q). All the residual phase variations we observe after removing these three terms is treated as noise (ϕ_M and ϕ_N). The ν and $\dot{\nu}$ measured for each of the two harmonics are given in Tables 1 and 2, respectively. The 68% confidence intervals on the pulse frequency and its derivative are calculated performing 10^4 MC simulations as described in Section 2. At long periods (days), red noise dominates the power spectrum, while at short periods (hours), the uncorrelated Poisson noise dominates. The red noise power spectrum is not very steep and has a power-law dependence $P(\nu) \propto \nu^{\alpha}$ with $\alpha \approx -0.5$. In Figure 1, we report the power spectrum of the fundamental and the second harmonics, after a constant $\dot{\nu}$ model has been subtracted from the pulse phases.

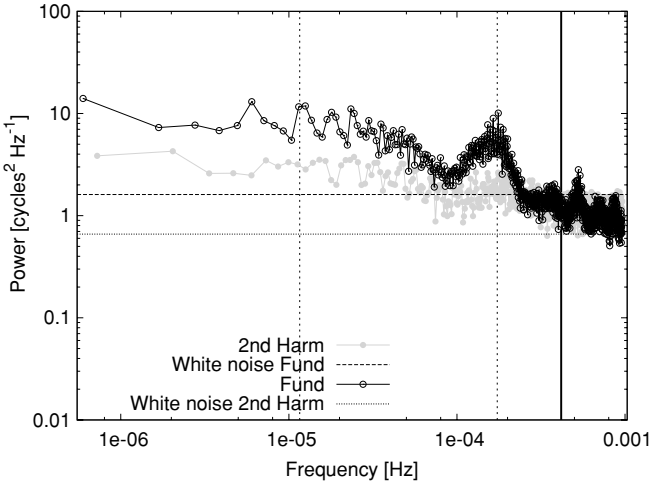

Figure 1. Power spectrum of the pulse phase residuals of the fundamental (black circles) and second harmonic (gray circles) obtained after subtracting a $\dot{\nu}$ model from the pulse phases. The horizontal dotted (for the fundamental) and dashed lines (for the second harmonic) refer to the white noise level given by the counting statistics. The two dashed vertical lines refer to the ≈1 day *RXTE* observing schedule and to the 96 minute *RXTE* orbit. The solid vertical line is the frequency that corresponds to the orbital period of the binary (∼40 minutes). The second harmonic presents no excess noise at the binary orbital frequency, while the fundamental has an excess noise of a factor of ∼1.8.

The source position we used comes from *Chandra* observations whose 68% confidence level error circle is 0.″4 in radius. The astrometric uncertainty introduced in this way on the frequency and frequency derivative is 3×10^{-8} Hz and 0.7×10^{-14} Hz s^{-1}, respectively (calculated with Equations (A1) and (A2) from Hartman et al. (2008), which, added in quadrature to the MC statistical errors, gives the final errors reported in Tables 1 and 2. The final pulse frequency derivative significances for the fundamental and the second harmonic are $\approx 2.7\sigma$ and $\approx 1.5\sigma$, respectively.

We note that the significance of the frequency derivative for the fundamental frequency increases above the 3σ level when the statistical errors are calculated with standard χ^2 minimization techniques, consistently with Riggio et al. (2008). These errors calculated with $\Delta\chi^2 = 1.0$ are 2×10^{-16} Hz s^{-1} and 1.6×10^{-15} Hz s^{-1} for the fundamental and second harmonics, respectively. So, a significant $\dot{\nu}$ is present which is, however, consistent with being part of the (red) timing noise. This means

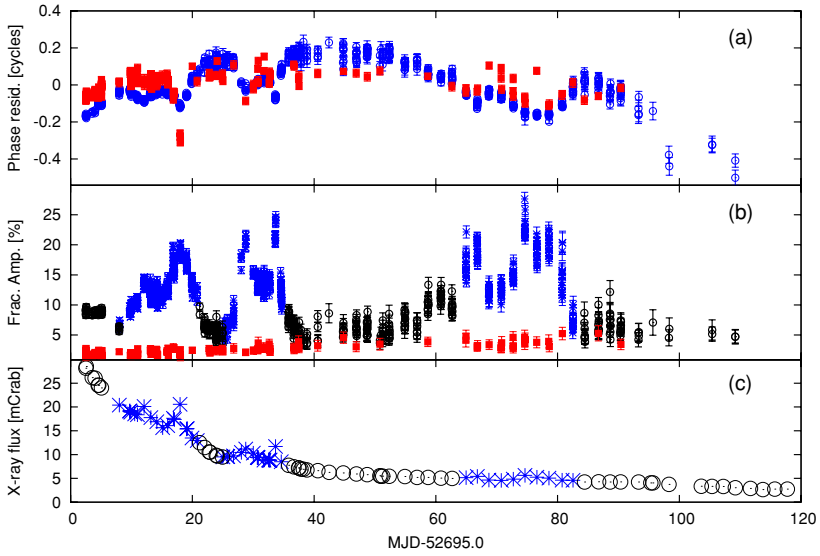

Figure 2. (a) Timing residuals for a constant spin frequency and a circular Keplerian orbit. The fundamental (blue circles) and the second harmonic (red squares) phases were measured using an integration time of 512 s per pulse profile. (b) Sinusoidal fractional amplitude of the fundamental (blue asterisks: flaring; black circles: non-flaring) and second harmonic (red squares) during the whole outburst. During the flares, the fundamental sinusoidal fractional amplitude grows up to ≈27%, which is the highest value ever observed for an AMXP. (c) XTE J1807−294 light curve of the 2003 outburst. The count rate was normalized to the Crab (Kuulkers et al. 1994) using the data nearest in time and in the same PCA gain epoch (e.g., van Straaten et al. 2003). The black circles and the blue asterisks identify the four non-flaring and the three flaring states, respectively, as defined in Chou et al. (2008).

(A color version of this figure is available in the online journal.)

Table 3
Timing Parameters for XTE J1807−294 (Fundamental)

Parameter	Fundamental	$\Delta\chi^2 = 1$ Error
Orbital period (s)	2404.4163	0.0003
Projected semimajor axis (lt-ms)	4.830	0.003
Time of ascending node (MJD)	52720.675601	0.000003

that our quadratic ϕ_Q component might be affected by the presence of red phase noise and thus all or part of it has to be included in the ϕ_N component.

The timing residuals obtained after removing a Keplerian circular orbit plus a $\dot{\nu} = 0$ model are plotted in Figure 2 for both harmonics (see Tables 1 and 2 for the pulse frequencies used in the fits). The fit gives a $\chi^2/\mathrm{dof} = 44,523.67/765 = 58.2$ and $\chi^2/\mathrm{dof} = 2322.9/142 = 16.36$ for the fundamental and second harmonics, respectively. These high values of the χ^2 reflect the high amount of timing noise at low frequencies. Our orbital solution is consistent for the two harmonics and with the orbital parameters published in Riggio et al. (2007). For the fundamental, we find the parameters reported in Table 3, where the quoted errors are calculated with the χ^2 minimization technique and correspond to $\Delta\chi^2 = 1$. Since the pulse phase residuals are approximately white and consistent with the expected Poissonian uncertainty, on timescales equal to and shorter than the orbital period, the orbital parameter errors are a good approximation of the true uncertainties and are not substantially affected by the timing noise (see Hartman et al. 2008 for a similar discussion on the orbital parameter uncertainties of SAX J1808.4−3658). In particular, the statistical errors of the second harmonic present no excess with respect to the white noise level, while the fundamental show a small excess on the order of 1.8 (see Figure 1).

3.2. Relation Between Timing Residuals and X-ray Flux

In this section, we analyze the relation between the pulse arrival time residuals relative to a constant pulse frequency ($\dot{\nu} = 0$) model and X-ray flux. Riggio et al. (2008) found that the residuals of the fundamental show a strong correlation with the X-ray flux, while the second harmonic shows only a marginal correlation. Since large pulse phase shifts are often observed (in both harmonics) in coincidence with the flaring states, we investigate the possibility that at least part of the observed timing noise is correlated with the presence of X-ray flux variations.

In this section, we show that both the harmonics are consistent with being correlated with X-ray flux. First, we focus on the entire data set, then we split the data into intervals choosing the same seven chunks as Chou et al. (2008; see also Figure 2(c)), distinguishing between the *non-flaring* states following the exponential flux decay of the overall outburst, and the *flaring* states comprising the six spikes in the light curve (see also Zhang et al. 2006 for a first identification of these intervals in the X-ray light curve). In Figure 3, we plot the residuals versus the count rate for both the fundamental and second harmonics.

We applied a Spearman rank correlation test to the flux anti-correlation for each harmonic. We accept the null hypothesis (no correlation in the data set) if the probability $p > 1\%$. If we do not make any data selection, the Spearman test shows no correlation in either harmonic. However, a clear split in the data is apparent at around 7 mCrab: below this threshold the residuals seem to follow a correlation with the flux, while above this threshold an anti-correlation is visible for both harmonics (see Table 4). A few outliers are visible in the plot, such as for example the four points of the second harmonic at about ≈ -0.3 cycles. These points correspond to the second harmonic for data taken during some of the flaring states.

The fact that we see a change from correlation to anti-correlation around 7 mCrab is due to the fact that at that flux level in the decay of the outburst the timing residuals reach the peak of the parabolic function that dominates the residuals (at MJD ≈ 52,745; see Figure 2). This is a consequence of the fitting procedure, which selects the constant reference pulse frequency that minimizes the χ^2 of the timing residuals. As the observed pulse frequency is increasing, the reference frequency

Table 4
Spearman Coefficients for the Flux–Residual Correlation

	Phase Fundamental	Phase Second Harmonic
Flux (all data points)	No correlation	No correlation
Flux (>7 mCrab)	−0.8	−0.65
Flux (only non-flaring state >7 mCrab)	−0.9	−0.76
Flux (only flaring state >7 mCrab)	−0.70	N/A
Flux (<7 mCrab)	+0.43	No correlation
Flux (only non-flaring state <7 mCrab)	+0.70	N/A
Flux (only flaring state <7 mCrab)	−0.31	N/A

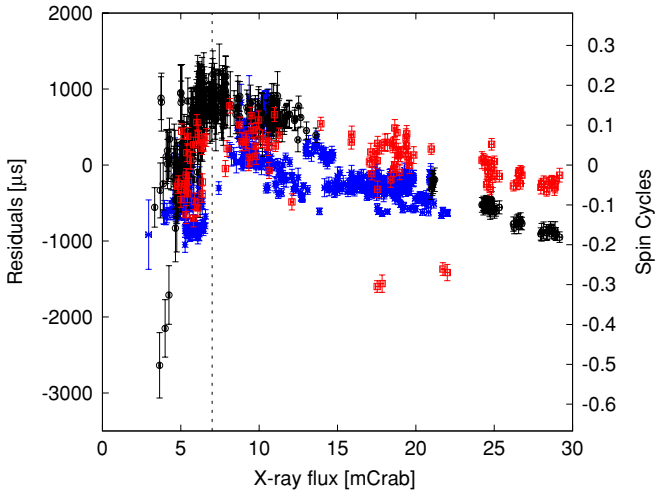

Figure 3. Phase residuals vs. X-ray flux for the fundamental (blue asterisks for the flaring intervals and open black circles for the non-flaring intervals) and the second harmonic (red open squares) relative to a $\dot{\nu} = 0$ model. Each pulse is a 512 s folded chunk of light curve. The dashed line at around 7 mCrab splits the diagram into two regions: in the left one the points follow a correlation, in the right one they follow an anti-correlation. The four points of the second harmonic that lay outside the relations correspond to the large jump observed during the second flare.

(A color version of this figure is available in the online journal.)

is too fast for the rising part of the residuals and too slow for the decreasing part.

We have seen in Section 3.1 that the measured pulse frequency increase is consistent with being part of a red noise process and that true neutron star spin variations may or may not be the cause. We can choose a higher reference pulse frequency than the one used to produce Figure 2(a), and turn the correlation–anti-correlation dichotomy in the flux-residual diagram into only an anti-correlation, at the cost of increasing the χ^2 of the pulse phases $\dot{\nu} = 0$ model by a factor of ≈10. This huge increase of the χ^2 is expected since we are now selecting the pulse frequency that maximizes the flux-residual anti-correlation instead of the pulse frequency that minimizes the pulse phase residuals in the fit with TEMPO.

We used frequency steps of 10^{-8} Hz and searched 500 frequencies around the pulse frequency reported in Tables 1 and 2. A ν higher than the frequencies reported in Tables 1 and 2 by 10^{-7} Hz makes the split in the data disappear and increases the degree of correlation between the flux and timing residuals. For a similar procedure applied to this source and to five other AMXPs, we refer to Patruno et al. (2009).

We also tried to select the best pulse frequency and pulse frequency derivative that maximizes the flux-residual anti-correlation instead of simply varying the pulse frequency. We scanned 2000 pulse frequency derivatives in the range $[-10^{-12}\,\mathrm{Hz\,s^{-1}}, +10^{-12}\,\mathrm{Hz\,s^{-1}}]$ and 500 pulse frequencies and found that the anti-correlation is maximized when the pulse frequency derivative is zero and the pulse frequency is still consistent with the same 10^{-7} Hz shift as found before.

All the correlations and anti-correlations disappear or are strongly reduced for the timing residuals relative to the best-fit finite constant-$\dot{\nu}$ model. However, after also removing a quadratic term from the light curve, the anti-correlations are observed again, with a similar degree of correlation as in the previous constant frequency model case. This is a hint that both long-term and short-term fluctuations are anti-correlated in a similar way. We recently confirmed this behavior in five more AMXPs (Patruno et al. 2009).

3.3. Harmonic Content and Amplitudes of Pulse Profiles

In this section, we focus on the harmonic content and the fractional amplitude of pulse profiles and their relation with other observables, such as the phase, the timing noise, and the X-ray flux.

3.3.1. The Fractional Amplitude-residual Diagram

We have seen in the previous section that for some data selections the X-ray flux correlates with the timing residuals relative to a $\dot{\nu} = 0$ model, but not when a constant $\dot{\nu}$ is admitted. As already noted by Zhang et al. (2006) and Chou et al. (2008), the fractional amplitude of the pulsations shows six spikes coincident with the six flares in the light curve. Therefore, a correlation might also exist between the fractional amplitude of the pulsations and the arrival time residuals. Using a $\dot{\nu} = 0$ model, and again using a Spearman rank test, we found a correlation for the fundamental frequency while no significant correlation exists for the second harmonic. Although no significant correlation is found for the second harmonic, we can still test whether its fractional amplitude and pulse phase residuals are consistent with following the same correlation found for the fundamental. We find that this is not the case: the fractional amplitudes of the second harmonic are inconsistent with being correlated with the phase residuals in the same way as the fundamental frequency. Repeating the test for a $\dot{\nu}$ model we still find no correlations for the second harmonic, but the anti-correlation found for the fundamental frequency becomes stronger. In Figure 4, we show the fractional amplitude versus residual diagram (relative to a $\dot{\nu}$ model). The anti-correlation is evident. It is interesting that the small number of points (circled in the figure) that are outliers all belong to the first 2.5 days of the outburst. We then analyzed the flaring and non-flaring states separately. The results are reported in Table 5.

We found no energy dependence in this fractional amplitude-timing residual anti-correlation (amplitude anti-correlation from now on) when we repeated the analysis in six different energy bands from 2.5 to 30 keV. The same is true for the second harmonic: no correlation was found in any energy band.

Table 5
Spearman Coefficients for the Fractional Amplitude–Residual Correlation

	Phase Fundamental	Phase Second Harmonic
Frac. Amp. ($\dot{\nu} = 0$ model; all data points)	−0.61	No correlation
Frac. Amp. ($\dot{\nu} = 0$ model; flaring state)	−0.58	N/A
Frac. Amp. ($\dot{\nu} = 0$ model; non-flaring state)	−0.43	N/A
Frac. Amp. ($\dot{\nu} =$ const model; all data points)	−0.80	No correlation
Frac. Amp. ($\dot{\nu} =$ const model; flaring state)	−0.81	N/A
Frac. Amp. ($\dot{\nu} =$ const model; non flaring state)	−0.51	N/A

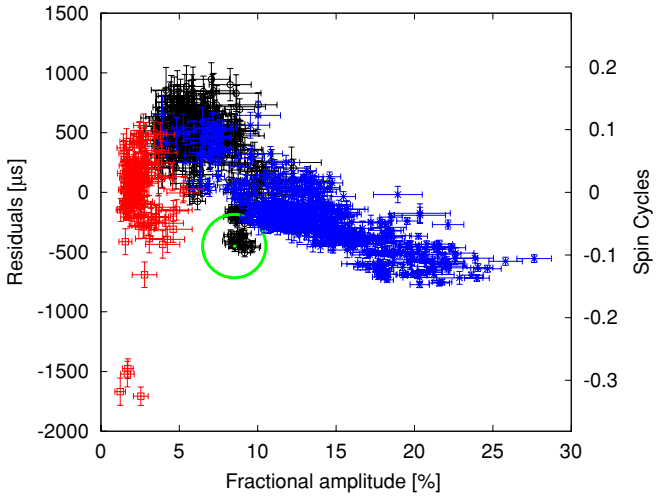

Figure 4. Timing residuals vs. fractional amplitude diagram. The blue asterisks refer to the flaring states, while the black circles are the non-flaring states, both referring to the fundamental frequency. The second harmonic is plotted as red open squares. Each pulse was built using 512 s of integration time. The residuals are relative to a constant $\dot{\nu}$ model. The green circled outliers of the anti-correlation for the fundamental all belong to the first 2.5 days of the observations. The second harmonic amplitude is uncorrelated with the timing residuals.

(A color version of this figure is available in the online journal.)

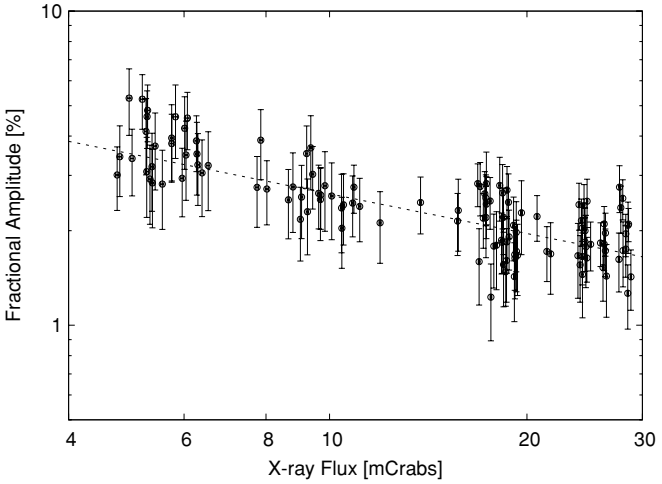

Figure 5. Fractional amplitude of the second harmonic is anti-correlated with the flux and scales with a power law of index $\gamma = -0.41 \pm 0.04$, close to the power-law index found in a similar relation for SAX J1808.4−3658.

3.3.2. The X-ray Flux and the Fractional Amplitude

In our previous paper (Hartman et al. 2008), we found an anti-correlation between the fractional amplitude of the second harmonic and the X-ray flux in SAX J1808.4−3658. We also noted that the fractional amplitude of the fundamental frequency behaved unpredictably. Something similar applies to J1807, where no correlation is found for the fundamental while a strong anti-correlation exists between the observed count rate and the fractional amplitude of the second harmonic ($\rho = -0.79$, $p < 1\%$, see Figure 5). The behavior of the fundamental is inconsistent with this relation. By analogy with Hartman et al. (2008) we fitted a simple power-law model ($R_2 \propto f_x^{\gamma}$, where f_x is the X-ray flux) to the data, which gives a power-law index $\gamma = -0.41 \pm 0.04$ with a χ^2/dof of 90.2/117. Interestingly, the power-law index we found for SAX J1808.4−3658 (Hartman et al. 2008) is in agreement with this. So, a difference in behavior exists between the fractional amplitude of the fundamental frequency and of the second harmonic. They respond differently to both the flux and the arrival time residuals.

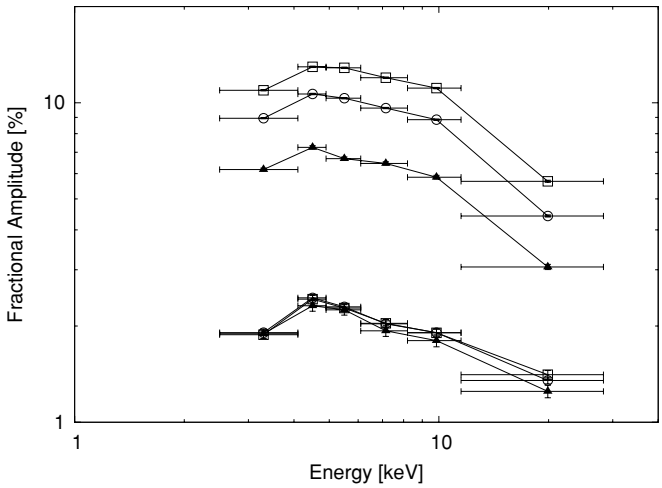

Figure 6. Energy dependence of the pulse fractional amplitudes. The squares and the triangles refer to the flaring and non-flaring states, respectively. The circles comprise the whole outburst. The bottom curves, overlapped in the plot, are the fractional amplitudes of the second harmonic, which remains stable in both states. The pulses of the fundamental in the flaring states have a fractional amplitude which is about 1.8 times larger than during the non-flaring states. Up to a constant factor, the fractional amplitude has the same energy dependence for both harmonics and for both flaring and non-flaring states.

3.3.3. Fractional Amplitude

We focus now on the energy dependence of the pulse profiles. We consider again all the data available and the subgroups of flaring and non-flaring states. Chou et al. (2008) already reported the energy dependence of the fundamental frequency during the non-flaring state. Here, we explore also the flaring state and the energy dependence of the second harmonic. Looking at Figure 6, two interesting features are immediately apparent.

1. The fractional amplitude energy dependence is the same for both harmonics regardless of the state of the source (flaring, non-flaring), up to a constant factor.

2. The fractional amplitude of the fundamental frequency increases by a factor of ≈1.8 during the flaring state with respect to the non-flaring state, while it remains approximately constant for the second harmonic.

Another important property of the pulses is the time dependence of the fractional amplitude. In the middle panel of Figure 2, we plot the fractional amplitude of the pulsations in the 2.5–30 keV band. As can be seen, during the last of the six flaring states the fractional amplitude of the fundamental frequency increases up to ≈27%, which is the highest ever observed for an AMXP. Selecting a narrower band between 2.5 and 10 keV, we find that the maximum fractional amplitude does not appreciably change. During the non-flaring stage, the fractional amplitude decreases smoothly from ≈9% down to ≈4%. The second harmonic amplitude on the contrary increases from ≈2% up to ≈5%.

3.3.4. Harmonic Content

We decomposed each pulse profile in its harmonic components to look for the presence of higher harmonics. While the detection of the second harmonic is quite common among the AXMPs, higher harmonics have never been detected, with the exception of a possible third harmonic in SAX J1808.4−3658 (Hartman et al. 2008). In J1807, we detected a third harmonic at better than 3σ, in several different stages of the outburst, with a maximum fractional amplitude of ≈1.5% at MJD around 52,560. To increase the signal-to-noise ratio (S/N), we folded chunks of data of length 3000 s. The number of $>3\sigma$ detections of the third harmonic was of 11 out of 163 chunks searched. We searched the same chunks for a fourth harmonic and found 5–10 significant detections above 3σ in the whole outburst, depending on the binning. When detected, the fourth harmonic has a fractional amplitude 0.5%–2.0%.

There were no observations where we detected all four harmonics at the same time. During the second and third flares, we found a second and fourth but not a third harmonic; during the first two flares we found a second and third but not a fourth harmonic.

For the third and fourth harmonics, we count, respectively, 8 and 5 detections during the flaring states and 3 and 2 detections in the non-flaring states.

The fractional amplitude of the third harmonic also decreases with the flux, although the slope of the power law is much smaller ($\gamma = -0.017 \pm 0.004$). The fourth harmonic has no significant flux dependence, but its power-law slope is also consistent with the γ obtained for the third harmonic.

Of course, this result has to be taken with caution, since we are suffering from low number statistics with only ≈20 detections of the third and fourth harmonics altogether. Furthermore, the analysis is suffering from a selection bias, since we are observing only those harmonics that appear with a sufficiently high S/N.

3.4. Short-term $\dot{\nu}$ Measurements

Using the fundamental frequency, we measured short-term pulse frequency derivatives using the seven subgroups of data as defined in Section 3.2. These measurements are useful to investigate the time dependence of the pulse frequency derivative with time. This test is possible in J1807 because of its very long outburst duration (more than 120 days, of which ≈106 days with detectable pulsations).

The $\dot{\nu}$ values and their uncertainties were first calculated with standard χ^2 minimization techniques. All measured $\dot{\nu}$ values during the non-flaring states had a positive sign, whereas a negative sign was measured for all three flaring states. The measured $\dot{\nu}$ values are shown in Figure 7. There is no clear trend, and most importantly no correlation between $\dot{\nu}$ and the average X-ray flux in either the flaring or the non-flaring states. This test cannot be performed on the second harmonic, since the smaller number of detections prevents a meaningful analysis of data subsets for this purpose.

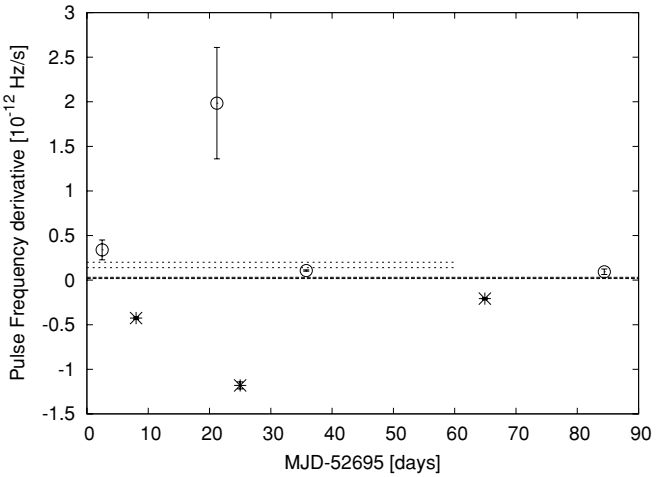

Figure 7. Pulse frequency derivative ($\dot{\nu}$) evolution. The non-flaring states (open circles) all have positive $\dot{\nu}$ that, however, does not follow a power-law decrease as expected from the accretion theory. The flaring states (asterisks) all have a negative value corresponding to spin down. The dotted and dashed lines are the 1σ confidence interval of the long-term $\dot{\nu}$ as reported by Chou et al. (2008; in the first 60 days) and Riggio et al. (2008): $1.7(3) \times 10^{-13}$ Hz s^{-1} and $2.4(7) \times 10^{-14}$ Hz s^{-1}, respectively.

We then calculated the statistical uncertainties on the $\dot{\nu}$ for each subgroup of data by using the MC method as explained in Section 3.1. All the $\dot{\nu}$ values were consistent with being part of the same red noise process, consistent with what was calculated for the long-term $\dot{\nu}$ value of Section 3.1. Therefore, a significant $\dot{\nu}$ is present on short timescales, which, however, is consistent with being part of the red timing noise.

We also plot in Figure 7 the results of the long-term $\dot{\nu}$ as measured by Riggio et al. (2008) and Chou et al. (2008): $2.4(7) \times 10^{-14}$ Hz s^{-1} and $1.7(3) \times 10^{-13}$ Hz s^{-1}, respectively. Particularly interesting is the measurement of Chou et al. (2008) which was performed only on the first 60 days of the outburst, discarding the remaining ∼30 days in which pulsations were still detectable. As we see from the figure, this particular choice makes the $\dot{\nu}$ deviate from the $\dot{\nu}$ of Riggio et al. (2008) and also from our confidence interval for $\dot{\nu}$ as reported in Section 3.1. The $\dot{\nu}$ of Chou et al. (2008) is consistent with the average value of the first five points of our short-term $\dot{\nu}$ measurements (which span ∼60 days of data, see Figure 7). This clearly shows that selecting subsets of data returns results for $\dot{\nu}$ that strongly depend on the particular choice of the data subset.

4. DISCUSSION

We have analyzed the outburst of XTE J1807−294 and we have calculated statistical errors by means of MC simulations as we previously did for SAX J1808.4−3658 (Hartman et al. 2008). We found that with our statistical treatment of the red noise observed in the timing residuals of both the fundamental and the second harmonics, the significance of the spin-up is reduced below 3σ for both the fundamental and the second harmonics.

The fact that the pulse frequency derivative is not significant does not mean that there is no quadratic component $\phi_Q(t)$ in the residuals that can be fitted with a parabola. It just means that the parabola (ϕ_Q) is consistent with having the same origin as the power at other low frequencies (ϕ_N): both the parabola and the remaining fluctuations are consistent with being part of the realization of the same red noise process in the timing residuals. In other words, ϕ_Q and ϕ_N are consistent with having the same origin. It is a separate issue whether or not this process is due to true spin changes and torques on the neutron star.

Our observed parabola ϕ_Q in the timing residuals combined with the stochastic ϕ_M and astrometric ϕ_A uncertainty implies that the value of any true spin frequency derivative has typical upper limits of $|\dot{\nu}| \lesssim 4 \times 10^{-14}\,\mathrm{Hz\,s^{-1}}$ at the 95% confidence level.

Evidence against the spin-up interpretation of the phases comes from the lack of any correlation between the observed X-ray flux and the measured $\dot{\nu}$ (see Section 3.4). If standard accretion torque theory applies, then the magnetospheric radius (r_m) should decrease as the mass accretion rate $\dot{M}$ increases, following a power-law $r_m \propto \dot{M}^{-\alpha}$ when $r_m < r_{\rm co}$, with $\alpha = 2/7$ in the simplest case, where $r_{\rm co}$ is the corotation radius. This also implies that the instantaneous $\dot{\nu}$ has a power-law dependence on the mass accretion rate, and (when $r_m < r_{\rm co}$) it is

$$\dot{\nu} = \frac{\dot{M}\sqrt{GMr_m}}{2\pi I} \simeq 1.6 \times 10^{-13}\,\mathrm{Hz\,s^{-1}} \times \left(\frac{\dot{M}}{10^{-10} M_\odot\,\mathrm{yr^{-1}}}\right)\left(\frac{\nu}{\mathrm{Hz}}\right)^{-1/3}\left(\frac{r_m}{r_{\rm co}}\right)^{1/2}; \quad (4)$$

see Bildsten et al. (1997). Here, $\dot{M}$ is the average mass accretion rate, M is the neutron star mass, and I is the neutron star moment of inertia. We have observed no such correlation between the flux and the instantaneous pulse frequency derivative either in the flaring or in the non-flaring states. One possible explanation is that the X-ray flux is not a good tracer of the mass accretion rate. If the X-ray flux is a good tracer of the mass accretion rate, standard accretion theory does not apply and the most logical conclusion is that the observed timing residuals are not due to torques.

The possibility that the X-ray flux is not a good tracer of the mass accretion rate is a long standing issue in the X-ray binary pulsar field and has no simple solution. If the X-ray flux is completely unrelated to the mass accretion rate, then no conclusions can be drawn about the effect of the accretion on the pulse phase.

By using Equation (4) we can calculate the spin frequency derivative expected for J1807 from standard accretion theory, assuming a distance of 8 kpc and converting the average X-ray luminosity into an average mass transfer rate through $L_x \approx \eta c^2 \dot{M}$. We assume an efficiency $\eta = 0.1$ for the conversion of gravitational potential energy into radiation. In this way, we obtain an average mass accretion rate $\dot{M} \approx 3 \times 10^{-11} M_\odot\,\mathrm{yr^{-1}}$ (averaging over the outburst). Assuming $r_m \approx r_{\rm co}$, we have an expected $\dot{\nu} \approx 10^{-14}\,\mathrm{Hz\,s^{-1}}$, which is within our calculated confidence interval of $(+0.7, +4.7) \times 10^{-14}\,\mathrm{Hz\,s^{-1}}$ and $(-0.6, +3.8) \times 10^{-14}\,\mathrm{Hz\,s^{-1}}$. However, the short-term $\dot{\nu}$ values calculated in Section 3.4 exceed the theory value by 1–2 orders of magnitude and therefore are very unlikely due to accretion torques.

The possibility that we are not observing the effect of a torque on the neutron star is also suggested by the fact that looking at the shape of the light curve, one can immediately infer the sign of the measured pulse frequency derivative in the timing residuals. This is a consequence of the flux anti-correlation. If the light curve is concave, then the average $\dot{\nu}$ is positive, while if the light curve has a convex shape, then the average $\dot{\nu}$ will be negative. This explains why $\dot{\nu} > 0$ in the non-flaring states and $\dot{\nu} < 0$ in the flaring states. It suggests a direct influence of the accretion rate on the phase, which could be effectuated through the hot spot position on the neutron star surface. Extending this interpretation to the average $\dot{\nu}$ over the entire outburst, we also favor the interpretation of a moving hot spot for that long-term trend, discarding the hypothesis of a torque to explain the parabolic ϕ_Q term observed in the pulse phase residuals.

Chou et al. (2008) also suggested that the lagging arrival times observed during the flaring states cannot be explained with a torque model, since they correspond to a sudden change from a spin-up to a spin-down. These authors also suggested that motion of the hot spot can be responsible for both the phase shifts and the increase of the fractional amplitude during the flaring states. Chou et al. (2008) assumed a fixed position of the hot spot during the non-flaring states. However, it is unlikely that the hot spot is fixed on the surface during the non-flaring state, as we have shown (see Section 3.4) that the magnitude of the short-term $\dot{\nu}$ is too large to be compatible with standard accretion theory.

Ibragimov & Poutanen (2009) recently proposed a receding disk as a possible explanation for the timing noise and pulse profile variability observed in the 2002 outburst of SAX J1808.4−3658. In this model, the antipodal spot can be observed when the inner accretion disk moves sufficiently far from the neutron star surface as a consequence of decreasing flux. We observed pulse phase drifts and a strong overtone from the early stages of the outburst, when the disk should be closest to the neutron star. Therefore, it is not clear whether our observations can be explained by this model or not, and further investigations of the problem are required.

Two hot spots with different and variable intensities can produce a phase shift and a changing pulsed amplitude, even if the location of both hot spots is fixed on the neutron star surface (Burderi et al. 2008). This possibility also needs further investigation since a self-consistent model has not yet been presented.

We observed (1) a relation between flux and TOAs for both the flaring and non-flaring states (Section 3.2). This relation was consistent with being the same for the two states. We also observed (2) an anti-correlation between pulse fractional amplitudes and TOAs during the flaring state. Finally, (3) this amplitude anti-correlation became stronger when using a long-term $\dot{\nu}$. The amplitude anti-correlation was weak in the non-flaring state, regardless of the $\dot{\nu}$. In the context of a hot spot motion model for the TOA variations, these findings constrain the kinematics of this motion.

Lamb et al. (2009) demonstrated that variations in the pulse fractional amplitudes should be anti-correlated with their TOA if the hot spot is close to the neutron star spin axis and the hot spot wanders by a small amount in latitude. Lamb et al. (2009) showed that even a small displacement in longitude of the emitting region, when close to the spin axis, produces a large phase change, but no amplitude variation. A motion in latitude produces both phase and amplitude changes due to the hot spot velocity variation affecting Doppler boosting and aberration. An anti-correlation between the pulse arrival times and the pulse amplitudes would be an indicator of the above.

Combining this with our observational findings (1)–(3) above, we conclude within the moving hot spot model for the phase variation that

1. The putative hot spot moves with flux in both flaring and non-flaring states, since the relation between flux and arrival times is observed in both cases and is consistent with being the same.
2. The amplitude anti-correlation in the flaring state implies a hot spot moving in latitude. The hot spot cannot move mainly in latitude during the non-flaring state since a weak amplitude anti-correlation is observed and the fractional amplitude changes by only a factor of $\approx$2 in 106 days.
3. The long-term $\dot{\nu}$ must be related to a motion in longitude since during the flaring state, the amplitude anti-correlation becomes much stronger when a $\dot{\nu}$ model is used to fit the TOAs. This is also compatible with the non-flaring state, since the amplitude anti-correlation remains weak with or without a $\dot{\nu}$.
4. Finally, a motion in longitude during the flaring state or in latitude during the non-flaring state is possible, but it has to be small enough to preserve the observed flux and amplitude anti-correlations.

The reason why the hot spot should drift mainly in longitude during the non-flaring states and mainly in latitude during the flares might be related to the differences in the accretion flow process. A hot spot motion has been observed in MHD simulations, with a complicated dependence of the hot spot position on the misalignment angle between the magnetic field and the rotation axis (Romanova et al. 2002, 2003, 2004). As noted by Lamb et al. (2009), long-term wandering of the hot spot can be related to the structure in the inner part of the accretion disk and therefore should track the long-term changes of the accretion rate. The position of the hot spot on the neutron star surface is expected to change rapidly and irregularly as the accretion flow from the inner region of the accretion disk varies. Further studies are required to couple our inferred hot spot kinematics to the physics and geometry of the accretion flow. We note that the fractional amplitudes can also change according to the hot spot angular size and/or to the difference in temperature between the hot spot and the neutron star surface.

The maximum observed sinusoidal fractional amplitude (Figure 2: $\approx$27%) can be explained if the hot spot is slightly misaligned from the spin axis (colatitude $\lesssim$20°) with an inclination of the observer larger than $\approx$45°, or if the inclination of the observer is smaller than $\approx$45° but the spot has a large colatitude (see Figure 4 in Lamb et al. 2009; note that we quote sinusoidal amplitudes while they use rms amplitudes).

J1807 shows an anti-correlation between the second harmonic fractional amplitude and the X-ray flux. We observed a similar anti-correlation in SAX J1808.4−3658 (Hartman et al. 2008). This suggests the same process as the origin of the anti-correlation in both pulsars. Hartman et al. (2008) found that the anti-correlation was a signature of the increasing asymmetry of the pulse profiles toward the end of the outburst. In J1807, the second harmonic is less often detected in these late stages of the outburst. However, the lower count rates late in the outburst lead to upper limits on the second harmonic that are sufficiently high such that the explanation we proposed for J1808 (Hartman et al. 2008) can still be valid for J1807 as well.

5. CONCLUSIONS

In this paper, we analyzed the 2003 outburst of XTE J1807−294 and found that the pulse frequency derivative previously reported in the literature is consistent with being part of a red noise process. No significant spin frequency derivative is detected when considering this red timing noise as a source of uncertainty in the calculation of statistical uncertainties, and 95% confidence intervals of $|\dot{\nu}| \lesssim 4 \times 10^{-14}\,\mathrm{Hz\,s^{-1}}$ for the fundamental and second harmonics can then be set for any spin frequency derivative. The average accretion torque expected from standard accretion theory predicts a long-term spin frequency derivative that is still compatible with the reported confidence intervals and cannot therefore be excluded from current observations.

We propose hot spot motion on the neutron star surface as a simpler model able to explain all the observations reported in this work, as well as the presence of a pulse frequency derivative. If this explanation is correct, similar flux and amplitude anti-correlations should be observed in other AMXPs.

We thank A. L. Watts, P. Casella, D. Altamirano, F. Lamb, S. Boutloukos, C. Miller, J. Poutanen, and C. Germaná for stimulating discussions.

REFERENCES

Bildsten, L., et al. 1997, ApJS, 113, 367
Boynton, P. E., & Deeter, J. E. 1985, in Proc. Inuyama Workshop on the Timing Studies of X-ray Sources, ed. S. Hayakawa & F. Nagase (Nagoya: Nagoya Univ.), 13
Burderi, L., Di Salvo, T., Riggio, A., Papitto, A., & Menna, M. T. 2008, in AIP Conf. Proc. 1068, A Decade of Accreting Millisecond X-ray Pulsars, ed. R. Wijnands et al. (Berlin: Springer), 17
Burderi, L., et al. 2006, ApJ, 653, L133
Chou, Y., et al. 2008, ApJ, 678, 1316
Groth, E. J. 1975, ApJS, 29, 443
Hartman, J. M., Patruno, A., Chakrabarty, D., Markwardt, C. B., Morgan, E. H., van der Klis, M., & Wijnands, R. 2009, ApJ, 702, 1673
Hartman, J. M., et al. 2008, ApJ, 675, 1468
Ibragimov, A., & Poutanen, J. 2009, MNRAS, 400, 492
Jahoda, K., et al. 2006, ApJS, 163, 401
Kuulkers, E., et al. 1994, A&A, 289, 795
Lamb, F. K., et al. 2009, ApJ, 706, 417
Markwardt, C. B., Smith, E., & Swank, J. H. 2003, ATel, 122, 1
Papitto, A., et al. 2007, MNRAS, 375, 971
Patruno, A., Altamirano, D., & Messenger, C. 2010, MNRAS, 403, 1426
Patruno, A., Wijnands, R., & van der Klis, M. 2009, ApJ, 698, L60
Poutanen, J. 2006, Adv. Space Res., 38, 2697
Riggio, A., di Salvo, T., Burderi, L., Iaria, R., Papitto, A., Menna, M. T., & Lavagetto, G. 2007, MNRAS, 382, 1751
Riggio, A., et al. 2008, ApJ, 678, 1273
Romanova, M. M., et al. 2002, ApJ, 578, 420
Romanova, M. M., et al. 2003, ApJ, 595, 1009
Romanova, M. M., et al. 2004, ApJ, 610, 920
Taylor, J. H. 1992, Phil. Trans. R. Soc., 341, 117
van Straaten, S., van der Klis, M., & Méndez, M. 2003, ApJ, 596, 1155
Warwick, R. S., Turner, M. J. L., Watson, M. G., & Willingale, R. 1985, Nature, 317, 218
Wijnands, R. 2004, Nucl. Phys. B, 132, 496
Wijnands, R., & van der Klis, M. 1998, Nature, 394, 344
Zhang, F., et al. 2006, ApJ, 646, 1116